
Cross-Trajectory Representation Learning for Zero-Shot Generalization in RL

Bogdan Mazoure^{*†}

bogdan.mazoure@mail.mcgill.ca
McGill University, Quebec AI Institute

Ahmed M. Ahmed^{*†}

ahmedah@stanford.edu
Stanford University

Patrick MacAlpine[†]

patmac@gmail.com
Sony AI

R Devon Hjelm

devon.hjelm@microsoft.com
Université de Montréal, Quebec AI Institute,
Microsoft Research

Andrey Kolobov

akolobov@microsoft.com
Microsoft Research

Abstract

A highly desirable property of a reinforcement learning (RL) agent – and a major difficulty for deep RL approaches – is the ability to generalize policies learned on a few tasks over a high-dimensional observation space to similar tasks not seen during training. Many promising approaches to this challenge consider RL as a process of training two functions simultaneously: a complex nonlinear *encoder* that maps high-dimensional observations to a latent *representation* space, and a simple linear *policy* over this space. We posit that a superior encoder for zero-shot generalization in RL can be trained by using solely an auxiliary SSL objective if the training process encourages the encoder to map *behaviorally similar* observations to similar representations, as reward-based signal can cause overfitting in the encoder [32]. We propose Cross Trajectory Representation Learning (CTRL), a method that runs within an RL agent and conditions its encoder to recognize behavioral similarity in observations by applying a novel SSL objective to pairs of trajectories from the agent’s policies. CTRL can be viewed as having the same effect as inducing a pseudo-bisimulation metric but, crucially, avoids the use of rewards and associated overfitting risks. Our experiments ablate various components of CTRL and demonstrate that in combination with PPO it achieves better generalization performance on the challenging Procgen benchmark suite [12].

1 Introduction

Deep reinforcement learning (RL) has emerged as a powerful tool for building decision-making agents for domains with high-dimensional observation spaces, such as video games [29], robotic manipulation [25], and autonomous driving [24]. However, while deep RL agents may excel at the specific task variations they are trained on, learning behaviors that generalize across a large family of similar tasks, such as handling a variety of objects with a robotic manipulator, driving under a variety of conditions, or coping with different levels in a game, remains a challenge. This problem is especially acute in zero-shot generalization (ZSG) settings, where only a few sequential tasks are available to learn policies that are meant to perform well on different yet related tasks without further parameter adaptation. This problem setting highlights the fact that generalization often cannot be solved by more training, as it can be too expensive or impossible to instantiate all possible real-world deployment scenarios a-priori.

^{*}Equal contribution. [†]The author did part of the work for this paper while at Microsoft.

In this work, we aim to improve ZSG in RL by proposing a new way of training the agent’s *representation*, a low-dimensional summary of information relevant to decision-making extracted from the agent’s high-dimensional observations. Outside of RL, representation learning can help with ZSG, e.g. using unsupervised learning to obtain a representation that readily transfers to unseen classes in vision tasks [8, 40, 45]. In RL, unsupervised representation learning in the form of auxiliary objectives can be used to provide a richer learning signal over learning from reward alone, which helps the agent avoid overfitting on task-specific information [32]. However, to our knowledge, no unsupervised learning method used in this way in RL has thus far been shown to substantially improve performance in ZSG over end-to-end reward-based methods [e.g., 12].

We posit that using unsupervised (reward-free) learning to find representations that capture behavioral similarity across different trajectories will improve ZSG in RL. We note that the bisimulation framework [17] does this directly with rewards, optimizing an agent to treat states as behaviorally similar based on the expected reward, and this has been shown to help in visual generalization settings [49]. We expand on this framework to improve ZSG performance, using unsupervised learning to train an agent that recognizes behavior similarity in a reward-free fashion. To do so, we propose *Cross Trajectory Representation Learning (CTRL)*, which applies a novel self-supervised learning (SSL) objective to pairs of trajectories drawn from the agent’s policies. For optimization, CTRL defines a prediction objective across trajectory representations from nearby partitions defined by an online clustering algorithm. The end result is an agent whose encoder maps behaviorally similar trajectories to similar representations without directly referencing reward, which we show improves ZSG performance over using pure RL or RL in conjunction with other unsupervised or SSL methods.

Our main contributions are as follows:

- We introduce Cross Trajectory Representation Learning (CTRL), a novel SSL algorithm for RL that defines an auxiliary objective across trajectories, drawing samples for a SSL predictive task by leveraging assignments from an online clustering algorithm. Our approach is two-fold: (i) we first map all trajectories to the closest representative dynamic across trajectories and (ii) boost cross-predictivity between samples of adjacent dynamic partitions.
- We empirically show that our cross-view auxiliary objective improves zero-shot generalization in the challenging Procgen benchmark suite [12]. Through a series of ablations, we highlight the importance of cross-trajectory views in boosting behavioral similarity.
- We connect CTRL to the class of bisimulation methods, and provide sufficient conditions under which both formalisms can be equivalent.

2 Background, motivation, and related works

There are a broad class of ZSG settings in RL, such as generalization across reward functions [7, 41, 28], observation spaces [49, 26, 32], or task dynamics [33]. For each of these settings, there are a number of promising directions for improving ZSG performance: giving the agent better exploration policies [43, 28, 1], meta learning [30, 20, 33], or planning [37]. In this work, we focus on the agent’s *representations*, because if the agent’s representations do not generalize well across tasks, one cannot expect its policy to readily do so. The tasks are assumed to share a common high-level goal and are set in environments that have the same dynamics, but each task may need to be accomplished under different initial conditions and may differ visually.

The agent’s *representations* are high-level abstractions of observations or trajectories from the environment (e.g., the output of an encoder), and the desired property here is that one can easily learn a policy on top of that representation such that the combined model (i.e., the agent) generalizes to novel situations. Unsupervised representation learning has been shown to improve generalization across domains, including zero-shot in vision [40, 45] and sample-efficiency in RL [16, 36, 39]. In RL, unsupervised objectives can be used as an *auxiliary objective* [or auxiliary task, 23], which provide an alternative signal to reward-based learning signal. Due to the potential role the RL loss may play in overfitting [32], we believe that separating learning objectives between the agent’s representation and its policy is crucial to guaranteeing good ZSG performance.

Self-supervised learning and reinforcement learning. A successful class of models that incorporate unsupervised objectives to improve RL use self-supervised learning (SSL) [3, 38, 27, 36, 39].

SSL formulates objectives by generating different *views* of the data, which are essentially transformed versions of the data, e.g., generated by using data augmentation or by sampling patches. While successful in their own way, prior works that combine SSL with RL do so by applying known SSL algorithms [e.g., from vision, 22, 42, 6, 11, 21, 19] to RL in a nearly off-the-shelf manner, predicting state representations *within* a given trajectory, only potentially using other trajectories as counterexamples in a contrastive loss. As such, these models provide no guarantees on generalization across RL tasks, potentially limiting their utility to ZSG.

Bisimulation metrics in reinforcement learning. Our hypothesis is that ZSG is achievable if the agent recognizes behavioral similarity between trajectories based on their long-term evolution. Learning this sort of behavior similarity is a central characteristic of bisimulation metrics [17], which assign a value of 0 to states which are behaviorally indistinguishable and have the same reward. Reward-based bisimulation metrics have been shown to learn representations that have a number of useful properties, e.g.: smoothness [18], visual invariance [49, 2] and multi-task adaptation [48]. For ZSG however, encoding relational information based on reward may not actually help [28, 41, 46], as the agent may overfit to spurious correlations between high-dimensional observations and the reward signal seen during training. HOMER [28] expands on the concept of bisimulation to learn behavioral similarity between states using unsupervised exploration at deployment. A recent thorough comparison of SSL and bisimulation frameworks also suggests that self-supervised objectives can outperform bisimulation-based algorithms on offline tasks [46]. CTRL expands on bisimulation metrics in a different direction, learning unsupervised behavior similarity conditioned on trajectories provided by an online RL algorithm, which makes it suitable for ZSG where the parameters are fixed at deployment. CTRL does this by using a predictive SSL objective between representations of “similar” trajectories drawn from RL policies.

Mining views across unsupervised clusters. Central to CTRL is how it identifies behavioral similarity between situations an RL agent encounters in an unsupervised way. First, it uses online clustering akin to [4] and Caron et al. [SwAV, 9] to group representations of trajectories, iteratively refining a partitioning of the latent space into regions of behavioral similarity. CTRL thereby explicitly finds unsupervised bisimulation relations for sets of trajectories, to which each trajectory embedding can be mapped via hard cluster assignments. Note that clustering by itself might collapse the representation of a trajectory to one of the cluster centroids. If C cluster centroids are regarded as representing prototypical behaviors, the collapse would equate any trajectory to one of these C behaviors, even if it is not very similar to any of them and would be best viewed as a behavior mixture. This is undesirable from the generalization standpoint. Therefore, CTRL has a second step: drawing inspiration from Mine Your Own View [MYOW, 5], it selects (*mines*) representational nearest neighbors from different, nearby clusters and applies a predictive SSL objective to them. This objective encourages their representations to be more similar and prevents representational collapse by pulling trajectory representations away from the centroids of their own assigned clusters. In RL, Proto-RL [47] also uses clustering to obtain a pre-trained set of prototypical states, but for a different purpose – to estimate state visitation entropy in hard exploration problems.

3 Problem statement and preliminaries

Formally, we define our problem setting w.r.t. a discrete-time Markov decision process (MDP) $M \triangleq \langle \mathcal{S}, \mathcal{A}, \mathcal{P}, \mathcal{R} \rangle$, where \mathcal{S} is a state space, \mathcal{A} is an action space, $\mathcal{P} : \mathcal{S} \times \mathcal{A} \times \mathcal{S} \rightarrow [0, 1]$ is a transition function characterizing environment dynamics, and $\mathcal{R} : \mathcal{S} \times \mathcal{A} \rightarrow \mathbb{R}$ is a reward function. M ’s state and action spaces may be discrete or continuous, but in the rest of the paper we assume them to be discrete to simplify exposition. In practice, an agent usually receives observations but not the full information about the environment’s current state. Consider an observation space \mathcal{O} and an observation function $\mathcal{Z} : \mathcal{S} \times \mathcal{O} \rightarrow [0, 1]$ that define what observations an agent may receive and how these observations are generated (possibly stochastically) from M ’s states. We define a *task* T as a partially observable MDP (POMDP) $T = \langle \mathcal{S}, \mathcal{A}, \mathcal{P}, \mathcal{R}, \mathcal{O}, \mathcal{Z}, s_0 \rangle$, where $s_0 \in \mathcal{S}$ is an initial state. Although many RL agents make decisions in a POMDP based only on the current observation o_t or at most a few recent ones, in general this may require using information from the entire observation history o_1, \dots, o_t so far. Denoting the space of such histories as \mathcal{H} , computing an agent’s behavior for task T amounts to finding a policy $\pi : \mathcal{H} \times \mathcal{A} \rightarrow [0, 1]$ with the optimal or near-optimal expected return from the initial state $V_T^\pi \triangleq \mathbb{E} \left[\sum_{t=0}^{\infty} \gamma^t \mathcal{R}(S_t, \pi(H_t) \mid S_0 = s_0) \right]$, where

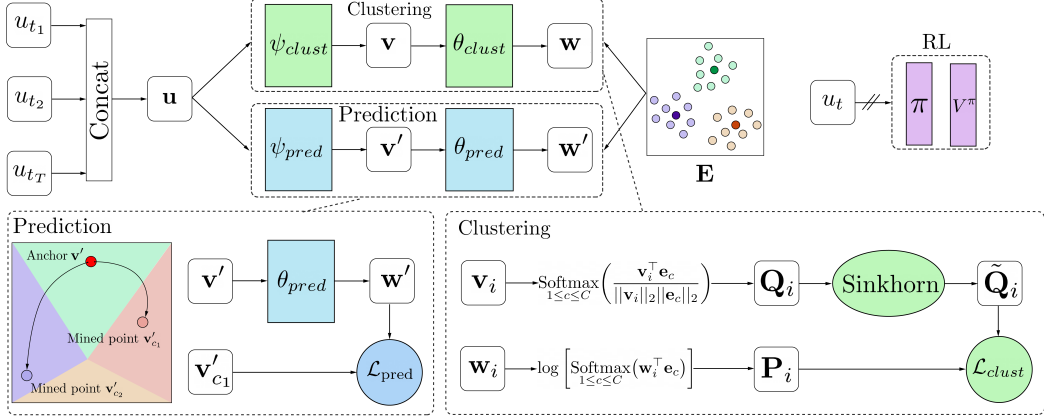


Figure 1: Schematic view of CTRL’s key components: a clustering procedure which finds groups of behaviorally similar states, and a prediction procedure to ensure that samples from a partition can be predicted from neighboring partitions.

S_t and H_t are random variables for the POMDP’s underlying state and agent’s observation history at time step t , respectively, and γ is a discount factor. For an MDP $M = \langle \mathcal{S}, \mathcal{A}, \mathcal{P}, \mathcal{R} \rangle$, a set \mathcal{O} of observation spaces, and a set \mathcal{Z} of observation functions w.r.t. \mathcal{S} , let a *task family* be the POMDPs set $\mathcal{T}_{M, \mathcal{O}, \mathcal{Z}} \triangleq \{\langle \mathcal{S}, \mathcal{A}, \mathcal{P}, \mathcal{R}, \mathcal{O}, \mathcal{Z}, s_0 \rangle\}_{\mathcal{O} \in \mathcal{O}, \mathcal{Z} \in \mathcal{Z}, s_0 \in \mathcal{S}}$. We assume that different observation spaces in \mathcal{O} have the same mathematical form, e.g., pixel tensors representing possible camera images, but correspond to qualitatively distinct subspaces of this larger space, such as subspaces of images depicting brightly and dimly lit scenes.

Our training and evaluation protocol is formalized w.r.t. a *task distribution* $d(\mathcal{T}_{M, \mathcal{O}, \mathcal{Z}}) \triangleq P(\mathcal{O}, \mathcal{Z}, \mathcal{S})$ over task family $\mathcal{T}_{M, \mathcal{O}, \mathcal{Z}}$, where $P(\mathcal{O}, \mathcal{Z}, \mathcal{S})$ is a joint probability mass over observation spaces, observation functions, and initial states. In the rest of the paper, M , \mathcal{O} , and \mathcal{Z} will be clear from context, and we will denote the task family as \mathcal{T} and the task distribution as $d(\mathcal{T})$. For agent training, we choose N tasks from \mathcal{T} , and denote the distribution $d(\mathcal{T})$ restricted to these N tasks as $d(\mathcal{T}_N)$. During the training phase, the RL agent learns via a series of epochs (themselves composed of episodes), by sampling a task from $d(\mathcal{T})$ independently at the start of each episode, until the total number of time steps exceeds its training budget. In each epoch, an RL algorithm uses a batch of trajectories gathered from episodes in order to compute gradients of an RL objective and update the parameters of the agent’s policy π . In representation learning-aided RL, a policy is viewed as a composition $\pi = \theta \circ \phi$ of an *encoder* $\phi : \mathcal{H} \rightarrow \mathcal{E}$ and a *policy head* $\theta : \mathcal{E} \times \mathcal{A} \rightarrow [0, 1]$, both of which are the outputs of the training phase. The training phase is followed by an evaluation phase, during which the policy is applied to tasks sampled from $d(\mathcal{T} \setminus \mathcal{T}_N)$, distribution d restricted to the set of tasks $\mathcal{T} \setminus \mathcal{T}_N$ not seen during training. *Our focus on generalization means that we seek a policy π whose encoder ϕ allows it to maximize $\mathbb{E}_{T \sim d(\mathcal{T} \setminus \mathcal{T}_N)}[V_T^\pi]$ despite being trained only on distribution $d(\mathcal{T}_N)$.*

4 Algorithm

CTRL’s key conceptual insight is that capturing behavioral similarity in a way that is agnostic to reward encourages ZSL because it enables ϕ to correctly associate previously unseen observation histories to those for which the agent’s RL-trained behavior applies a good action. CTRL runs synchronously with an online RL algorithm, which is crucial to ensure that as the agent’s policies improve, so does the notion of behavioral similarity induced by CTRL. Like most online RL methods themselves, our algorithm operates in epochs, learning from a batch of trajectories in each epoch. Before the RL algorithm updates the policy head θ over the epoch’s trajectory batch, CTRL uses this trajectory batch to update the encoder ϕ with 4 operations:

1. Apply ϕ and additional projections to stochastically generate a low-dimensional *reward-agnostic* view of each trajectory from the batch.

2. Group the trajectory views with the clustering procedure into C partitions, where C is CTRL's hyperparameter. Compute a clustering loss $\mathcal{L}_{\text{clust}}$.
3. Sample pairs of trajectories whose views are in nearby clusters. For each trajectory in a pair, construct its mined view. Compute a prediction loss $\mathcal{L}_{\text{pred}}$ over the mined views of the chosen trajectory pairs.
4. Update ϕ , cluster centroids, and other parameters involved in computing the views w.r.t. the CTRL objective $\mathcal{L}_{\text{CTRL}} = \mathcal{L}_{\text{clust}} + \mathcal{L}_{\text{pred}}$.

We refer the reader to CTRL's pseudocode in Algorithm 1 (Appendix) and the schema in Figure 1. While in general the agent's belief state at step t of a trajectory is the entire observation history $h_t = (o_1, \dots, o_t)$, in the rest of the section we will assume $h_t = (o_t)$ and, in a slight abuse of notation, use $\phi(o_t)$ instead of $\phi(h_t)$ to simplify explanations². We emphasize, however, that CTRL equally applies in settings where the agent uses the entire history of observations as its state.

Generating low-dimensional trajectory views with encoder ϕ . CTRL's input in each epoch is a trajectory batch $\{\text{traj}_i\}_{i=1}^B$ of size B . Assume all trajectories in the batch have the same length L . For an integer hyperparameter $T \leq L$, for each trajectory $\text{traj}_i = (o_0, a_0, r_0, \dots, o_{T_b}, a_L, r_L)$ we independently and uniformly sample a subset of its steps $\tau_i = t_1, \dots, t_T$ to form a subtrajectory $(o_{t_1}, a_{t_1}, r_{t_1}, \dots, o_{t_T}, a_{t_T}, r_{t_T})$. We then encode this subtrajectory as

$$\mathbf{u}_i^{(\tau_i)} = (\text{FiLM}(\phi(o_{t_1}), a_{t_1}), \dots, \text{FiLM}(\phi(o_{t_T}), a_{t_T})), \quad (1)$$

where $\text{FiLM}(\phi(o_{t_j}), a_{t_j})$ is a common way of combining representations of different objects, akin to conditioning [31], and the resulting vector $\mathbf{u}_i^{(\tau_i)}$ is in a low-dimensional space \mathcal{U} . Note two aspects of the process of generating these vectors: (1) it drops rewards from the original trajectory and (2) it critically relies on ϕ whose parameter values are learned from previous epochs. Vectors $\mathbf{u}_i^{(\tau_i)}$ produced in this way are the trajectory views that the next steps of CTRL operate on.

Clustering trajectory views. CTRL groups trajectories from the epoch's batch by clustering the set of their views $\{\mathbf{u}_i^{(\tau_i)}\}_{i=1}^B$ using the Sinkhorn procedure [9].

The clustering branch computes two views of each input $\mathbf{u}_i^{(\tau_i)}$ in a cascading fashion: first by passing it through a clustering encoder $\psi_{\text{clust}} : \mathcal{U} \rightarrow \mathcal{V}$, e.g. an RNN, to obtain a lower-dimensional view $\mathbf{v}_i = \psi_{\text{clust}}(\mathbf{u}_i^{(\tau_i)})$, and then by passing \mathbf{v}_i through yet another network, an MLP $\theta_{\text{clust}} : \mathcal{V} \rightarrow \mathcal{W}$, to produce view $\mathbf{w}_i = \theta_{\text{clust}}(\mathbf{v}_i)$. The parameters of ψ_{clust} and θ_{clust} are learned through the epochs jointly with ϕ 's. Like $\mathbf{u}_i^{(\tau_i)}$, each \mathbf{v}_i and \mathbf{w}_i is a view of trajectory i ; the approach then consists in projecting \mathbf{v}_i 's and \mathbf{w}_i 's onto centroids of C clusters in two different ways and then computes a clustering loss that enforces consistency between \mathbf{v}_i 's and \mathbf{w}_i 's cluster projections.

Specifically, we represent the centroid of each cluster c with a vector $\mathbf{e}_c \in \mathcal{V}$, which are stacked into a matrix \mathbf{E} . These vectors are additional parameters in the joint optimization problem CTRL solves. They can be regarded as views of C typical behaviors around which the trajectories' views are regrouped. To project trajectory i 's \mathbf{v}_i views onto behavioral centroids learned from previous trajectory batches, CTRL computes a vector of soft assignments of \mathbf{v}_i to each centroid \mathbf{e}_c :

$$\mathbf{Q}_i = \text{Softmax}_{1 \leq c \leq C} \left(\frac{\mathbf{v}_i^\top \mathbf{e}_c}{\|\mathbf{v}_i\|_2 \|\mathbf{e}_c\|_2} \right) \quad (2)$$

and forms a $B \times C$ matrix \mathbf{Q} whose i -th row is the soft assignment of \mathbf{v}_i . The resulting assignments may be very unbalanced, with most probability mass assigned to only a few clusters. Applying the Sinkhorn-Knopp algorithm solves this issue by iteratively re-normalizing \mathbf{Q} in order to obtain a more equal cluster membership [14], where the degree of re-normalization is controlled by a temperature parameter β . The output of this operation is a matrix $\tilde{\mathbf{Q}}$.

²While, in theory, the Procgen suite is indeed a POMDP, most practical applications treat it's belief state as being the most recent observation - a simplification which was shown not to hinder ZSG [12].

For each view \mathbf{w}_i , the projection of trajectory view \mathbf{v}_i , CTRL computes the logarithm of its soft cluster assignments:

$$\mathbf{P}_i = \log \left[\underset{1 \leq c \leq C}{\text{Softmax}}(\mathbf{w}_i^\top \mathbf{e}_c) \right], \quad (3)$$

and treats these vectors as rows of another $B \times C$ matrix \mathbf{P} .

Finally, we compute the cross entropy between $\tilde{\mathbf{Q}}$ and \mathbf{P} , which measures their inconsistency. This measure is taken as the clustering loss:

$$\mathcal{L}_{\text{clust}} = \text{CrossEntropy}(\tilde{\mathbf{Q}}, \mathbf{P}) \quad (4)$$

View mining for encouraging cross-cluster representation coherence. The clustering loss implicitly encourages views of trajectories from different clusters to be dissimilar. If it was the only factor driving the representation learning process, it would ultimately cause ϕ to map any observation history to one of a few small regions in the representation space \mathcal{E} , even if the given trajectory signature is not very close behaviorally to any trajectory seen during training. This would hurt rather than help generalization (see Appendix 8.3). CTRL prevents this by pushing ϕ and other components of CTRL’s workflow towards making views of trajectories from *nearby* clusters predictive of each other.

To implement this idea, we define a measure of cluster proximity via a matrix \mathbf{D} of cosine similarities between cluster centroids: for clusters k and l , $\mathbf{D}_{kl} = \|\mathbf{e}_k - \mathbf{e}_l\|_2^2$ [19]. Recall that in the previous step, the clustering branch computed a matrix \mathbf{Q} whose rows \mathbf{Q}_i are soft assignments of trajectory i ’s view \mathbf{v}_i to clusters. In this step, we convert these soft assignments to hard ones by associating a trajectory’s view \mathbf{v}_i with cluster $c_i = \text{argmax}_{1 \leq c \leq C} \mathbf{Q}_i$ and treating a cluster c as consisting of trajectories with indices in the set $\mathbb{T}_c = \{i \mid c = \text{argmax}_{1 \leq c \leq C} \mathbf{Q}_i\}$. To assess how predictive a trajectory embedding \mathbf{u}_i is of a trajectory embedding \mathbf{u}_j , like in the clustering step we will use two special helper maps, $\psi_{\text{pred}} : \mathcal{U} \rightarrow \mathcal{V}$ to obtain a reduced-dimensionality view $\mathbf{v}' = \psi_{\text{pred}}(\mathbf{u})$ and θ_{pred} to further project \mathbf{v}' to $\mathbf{w}' = \theta_{\text{pred}}(\mathbf{v}')$.

CTRL proceeds by repeatedly sampling trajectories, which we call *anchor trajectories*, from the batch, with their associated embeddings \mathbf{u} . For each anchor trajectory n , consider K clusters c_1, \dots, c_K nearest to n ’s cluster c_n , as defined by the indices of K largest values in row c_n of matrix \mathbf{D} (we exclude c_n itself when determining c_n ’s nearest clusters). Borrowing ideas from the MYOW approach [5], CTRL mines a view for \mathbf{u}_n by randomly choosing a trajectory with embedding $\mathbf{u}_{c_k}^{(n)}$ from each of the neighboring clusters and computing its view $\mathbf{v}'_{c_k} = \psi_{\text{pred}}(\mathbf{u}_{c_k}^{(n)})$. We call the neighbors’ views $\mathbf{v}'_{c_1}, \dots, \mathbf{v}'_{c_K}$ trajectory n ’s *mined views*.

For the final operation in this step, CTRL computes trajectory n ’s predictive view $\mathbf{w}'_n = \theta_{\text{pred}}(\psi_{\text{pred}}(\mathbf{u}_n))$ and measures the distance from it to trajectory n ’s mined views:

$$\mathcal{L}_{\text{pred}}^{(n)} = \sum_{k=1}^K \|\mathbf{w}'_n - \mathbf{v}'_{c_k}\|_2^2 \quad (5)$$

N is the CTRL’s hyperparameter that determines the number of anchor trajectories to be sampled, so the total prediction loss is

$$\mathcal{L}_{\text{pred}} = \sum_{n=1}^N \mathcal{L}_{\text{pred}}^{(n)} \quad (6)$$

Updating encoder ϕ . In the final step, CTRL computes its objective, a combination of the clustering and prediction losses:

$$\mathcal{L}_{\text{CTRL}} = \mathcal{L}_{\text{clust}} + \mathcal{L}_{\text{pred}} \quad (7)$$

Note that this loss depends on the parameters of encoder ϕ as well as of clustering networks ϕ_{clust} and θ_{clust} , prediction networks ϕ_{clust} and θ_{clust} , and cluster centroids \mathbf{e}_c , $1 \leq c \leq C$. In each epoch, CTRL updates all these parameters to minimize $\mathcal{L}_{\text{CTRL}}$.

5 Results

We compare CTRL against strong RL baselines: DAAC [32] – the current state-of-the-art on the challenging generalization benchmark suite *Procgen* [12], and PPO [35]. DAAC optimizes the PPO loss [35] through decoupling the training of the policy and value functions, which updates the advantage function during the policy network updates. We then compare to several unsupervised and SSL auxiliary objectives used in conjunction with PPO. DIAYN [16] is an unsupervised skill-based exploration method which we adapt to the online setting by uniformly sampling skills. Its notion of skills has some similarities to the notion of clusters in CTRL. We also compare with two SSL-based auxiliary objectives: CURL [38], a common SSL baseline which contrasts augmented instances of the same state; and Proto-RL [47], which we adapt for this generalization setting and denote PPO+Sinkhorn. Finally, we provide a comparison against a bisimulation-based algorithm, DBC [49], which was shown to perform well on robotic control tasks with visual distractor features.

The Procgen benchmark suite, which we use in our experiments, consists of 16 video games (see Table 1). Procgen procedurally generates distinct levels for each game. The number of levels for each game is virtually unlimited. Levels within a game which share common game rules and objectives but differ in level design such as the number of projectiles, background colors, item placements throughout the level and other game assets. The dynamics and rewards from a given Procgen level are shared with all other levels, while its observation space and the initial underlying state s_0 (about which the agent has no direct knowledge) is distinct. Moreover, the subspaces of the underlying state space \mathcal{S} that can be visited from s_0 ’s of different levels are largely disjoint. All of this makes Procgen a suitable benchmark for zero-shot generalization. Using our notation from Section 3, for each of 16 games, we train on a uniform distribution $d(\mathcal{T}_N)$ over $N = 200$ levels of the game and evaluate on $d(\mathcal{T} \setminus \mathcal{T}_N)$, i.e., a uniform distribution over the game’s levels not seen during training.

Table 1: Average evaluation returns collected after 8M training frames, \pm one standard deviation.

Env	RL		RL+Bisim.		RL+Unsup.		RL+SSL		Ours
	PPO	DAAC	PPO+DBC	PPO+DIAYN	PPO+Sinkhorn	PPO+CURL	CTRL		
bigfish	2.5 \pm 0.3	4.5 \pm 0.8	1.8 \pm 0.1	2.2 \pm 0.1	2.4 \pm 0.1	2.2 \pm 0.2	4.9\pm0.3		
bossfight	6.2 \pm 0.5	1.9 \pm 1.2	5 \pm 0.1	1.1 \pm 0.2	6.1 \pm 0.5	5.4 \pm 0.9	8.6\pm0.2		
cafeflyer	4.7 \pm 0.4	4.3 \pm 0.1	3.6 \pm 0.1	1.0 \pm 1.9	4.7 \pm 0.1	4.8\pm0.3	4.8\pm0.2		
chaser	7.5 \pm 0.2	7.3 \pm 0.1	4.8 \pm 0.1	5.6 \pm 0.5	7.6\pm0.2	7.4 \pm 0.1	7.3 \pm 0.2		
climber	5.8 \pm 0.1	5.8 \pm 0.4	4.1 \pm 0.4	0.8 \pm 0.7	5.7 \pm 0.4	5.7 \pm 0.4	6.2\pm0.2		
coinrun	8.3 \pm 0.2	8.2 \pm 0.2	7.9 \pm 0.1	6.4 \pm 2.6	8.2 \pm 0.1	8.1 \pm 0.1	8.7\pm0.4		
dodgeball	1.3 \pm 0.1	1.9\pm0.2	1.0 \pm 0.3	1.4 \pm 0.2	1.6 \pm 0.1	1.5 \pm 0.1	1.9\pm0.1		
fruitbot	12.7 \pm 0.2	12.6 \pm 0.2	2 \pm 0.2	7.2 \pm 3.0	12.3 \pm 0.4	13.1 \pm 0.4	13.5\pm0.3		
heist	2.9 \pm 0.2	3.4\pm0.2	3.3 \pm 0.2	0.2 \pm 0.2	3.0 \pm 0.3	2.6 \pm 0.3	3.3 \pm 0.3		
jumper	6.0 \pm 0.1	6.5\pm0.1	3.9 \pm 0.4	2.6 \pm 2.3	6.1 \pm 0.1	6.0 \pm 0.1	6.1 \pm 0.1		
leaper	3.3 \pm 0.9	3.8\pm0.6	2.7 \pm 0.1	2.5 \pm 0.2	3.2 \pm 0.8	3.8\pm0.9	2.6 \pm 0.3		
maze	5.5 \pm 0.2	5.7\pm0.3	5.0 \pm 0.1	1.6 \pm 1.2	5.5 \pm 0.3	5.5 \pm 0.1	5.7\pm0.1		
miner	8.8 \pm 0.3	6.3 \pm 0.6	4.8 \pm 0.1	1.3 \pm 2.0	8.8 \pm 0.5	8.9\pm0.1	6.8 \pm 0.2		
ninja	5.4 \pm 0.2	5.5 \pm 0.2	3.5 \pm 0.1	2.8 \pm 2.0	5.4 \pm 0.3	5.7 \pm 0.2	5.8\pm0.1		
plunder	6.2 \pm 0.4	4.0 \pm 0.2	5.1 \pm 0.1	2.1 \pm 2.5	6.0 \pm 0.9	6.7\pm0.2	6.7\pm0.4		
starpilot	5.2 \pm 0.2	4.7 \pm 0.4	2.8 \pm 0.1	5.8 \pm 0.6	5.2 \pm 0.2	5.2 \pm 0.2	7.9\pm0.5		

As Table 1 shows, PPO+CTRL outperforms all other baselines, including DAAC, on most games. Notably, bisimulation-based approaches other than CTRL exhibit lower gains than others. While this can be surprising, recent work has seen similar results when applying DBC to tasks with unseen backgrounds [26]. Even though training static prototypes for 8M timesteps and adapting the RL head for 8M additional timesteps, PPO+Sinkhorn (ProtoRL) performs worse than CTRL, suggesting that the temporal aspect of clustering is key for zero-shot generalization. Likewise, PPO+DIAYN uses its pre-training phase to find a diverse set of skills, which can be useful in robotics domains, but does not help much in the ZSG setting of Procgen. DAAC also exhibits good generalization performance, but inherits from PPG [13] the separation of the value and policy branches both parameter-wise and by introducing distinct training phases, an overhead which CTRL manages to avoid.

5.1 Slow clustering suggests good generalization

Finding cross-trajectory similarities with an unsupervised procedure heavily relies on the policy which collected the training samples. If the learning happens too quickly and the behavioral similarities are found early in the training procedure, such a representation will not be robust to distribution shifts induced by improved policies. Therefore, it is crucial to learn the behavioral similarities at a rate which allows the centroids to adapt to the value improvement path [15]. To validate this hypothesis, we conducted an analysis of the correlation between the clustering quality and the test performance on three representative games. To measure the clustering quality, we report the silhouette score [34], a commonly used unsupervised goodness-of-fit measure which balances inter- and intra-cluster variance. Results shown in Figure 2 provide evidence that picking the unsupervised learning procedure which converges the fastest (i.e. uses the lowest temperature β) does not necessarily lead to the best generalization performance. Based on Figure 2, we conjecture that fast clustering convergence hinders the performance of the RL agent due to clusters being fixed early on and not adapting to the evolving RL policy.

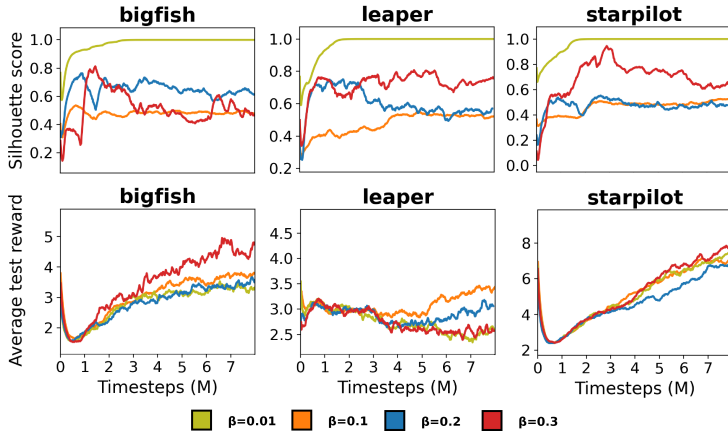


Figure 2: Goodness-of-clustering measured by silhouette scores (top) and average test returns (bottom) as a function of training samples.

5.2 Learning behavioral similarities captures local perceptual changes

To demonstrate the importance of trajectory view mining, a key component of our algorithm, we designed a toy example based on the standard Ising model³. The task relies on randomly initializing 5 Ising models, each parametrized by an inverse temperature parameter on a uniform grid $\beta \in [0.01, 0.3]$ and representing local behavior in the system. The agent is initialized in one of the 5 branches randomly, and, every timestep, receives feedback from the Ising model it is currently interacting with. The 5 actions allow the agent to swap out the current branch for any of the 5 available. The goal of the task is to match a pre-existing configuration that was obtained by evolving an Ising model with unknown parameters for a random number of timesteps. We additionally perturb all pixel observations with i.i.d. Gaussian noise to make the system less predictable. Figure 3 outlines the experimental setting for this study case.

Table 2 outlines the results we obtained by deploying our algorithm with different number of clusters

	$E = 2$	$E = 4$	$E = 5$	$E = 6$	$E = 50$
Returns	-0.78	-0.96	0.07	-0.02	-0.54
Silhouette	0.875	0.796	0.651	0.554	0.039
Silhouette change	-	0.079	0.145	0.097	0.515

Table 2: Returns and silhouette scores obtained by CTRL in the composite Ising matching domain.

³https://en.wikipedia.org/wiki/Ising_model

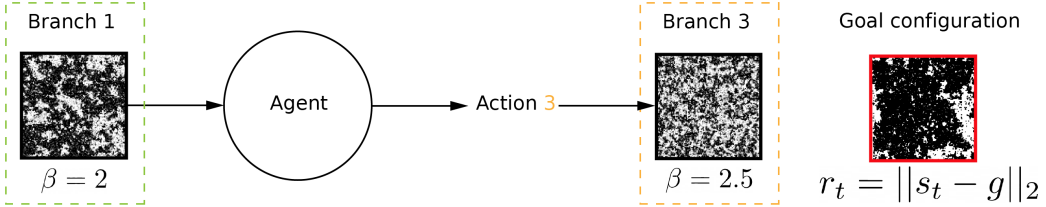


Figure 3: The composite Ising matching problem: the agent has to match a given Ising configuration by swapping branches of various transition dynamics

One can see that the largest improvement in silhouette score occurs from $E = 4$ to $E = 5$ (14.5%), suggesting that CTRL finds the correct number of clusters.

6 Connection to bisimulation

Deep bisimulation metrics are tightly connected to the underlying mechanism of mining behaviorally similar trajectories of CTRL. They operate on a latent-dimensional space and, as is the case for DeepMDP [18] and DBC [49], ensure that bisimilar states (i.e. behaviorally similar states with identical reward) are located close to each other in that latent space. In this section, we aim to highlight a functional similarity between bisimulation metrics and CTRL.

Definition 1 A bisimulation relation $E \subseteq \mathcal{S} \times \mathcal{S}$ is a binary relation which satisfies, $\forall (s, t) \in E$:

1. $\forall a \in \mathcal{A}, \mathcal{R}(s, a) = \mathcal{R}(t, a)$
2. $\forall a \in \mathcal{A}, \forall c \in \mathcal{S}, \sum_{s' \in c} \mathcal{P}(s, a)(s') = \sum_{s' \in c} \mathcal{P}(t, a)(s')$

In practice, rewards and transition probabilities rarely match exactly. For this reason, [17] proposed a smooth alternative to bisimulation relations in the form of bisimulation metrics, which can be found by solving a recursive equation involving the Wasserstein-1 distance \mathcal{W}_1 between transition probabilities. \mathcal{W}_1 can be found by solving the following linear programming [44], where we let $\Gamma = \{\mathbf{v} \in \mathbb{R}^{|\mathcal{V}|} : 0 \leq v_i \leq 1 \forall 1 \leq i \leq |\mathcal{V}|\}$:

$$\begin{aligned} \mathcal{W}_1^d(P||Q) := \max_{\mu \in \Gamma} \sum_{s \in \mathcal{S}} (P(s) - Q(s))\mu(s) \\ \text{s.t. } \mu(s) - \mu(s') < d(s, s') \forall s, s' \in \mathcal{S}, \end{aligned} \quad (8)$$

where μ is a vector whose elements are constrained between 0 and 1. In practice, bisimulation metrics are used to enforce a temporal continuity of the latent space by minimization of the \mathcal{W}_1 loss between training state-action pairs. Therefore, to show a connection of CTRL to (reward-free) bisimulation metrics, it is sufficient to show that two trajectories are mapped to the same partition if their induced \mathcal{W}_1 distance is arbitrarily small. In our (informal) argument that follows, we assume that CTRL samples two consecutive timesteps and encodes them into \mathbf{v} ; the exact form of \mathbf{v} dictates the nature of the behavioral similarity.

Proposition 1 (Informal) Let M be an MDP where $\mathcal{R}(s, a) = 0$ for all $(s, a) \in \mathcal{S} \times \mathcal{A}$ and let $\mathbf{v}, \mathbf{v}' \in \mathcal{V}$ be two dynamics embeddings in M . The clustering operation between \mathbf{v}, \mathbf{v}' induces a reward-free bisimilarity metric $\mathcal{W}_1(\mathbb{P}[\mathbf{v}], \mathbb{P}[\mathbf{v}'])$ between induced distributions $\mathbb{P}[\mathbf{v}]$ and $\mathbb{P}[\mathbf{v}']$.

The proof can be found in Appendix 8.5 and follows from a re-arrangement of terms in the matrix $\tilde{\mathbf{Q}}$.

7 Discussion

In this work, we proposed CTRL, a novel representation learning algorithm for RL that encourages zero-shot generalization across pixel-based observation spaces. CTRL operates synchronously with RL by choosing pairs of trajectories generated by the RL agent's learned behaviors, which are trained

directly by an RL algorithm. CTRL operates by grouping behaviorally similar trajectories together, which can in fact be viewed as inducing an unsupervised reward-agnostic bisimulation metric over observation histories, learned over transitions encountered by policies from an RL algorithm’s *value improvement path* [15]. Thus, as the agent’s policies become better, CTRL trains the encoder to match observations by similarities relevant to increasingly better behaviors. Notably, it is similar to the on-policy bisimulation as defined in Castro [10], which has been shown to benefit from better convergence properties due to operating with the current policy, as opposed to all possible policies, hence not focusing on worst-case behaviors.

Zero-shot generalization of RL algorithms is especially important for domains in which these methods are currently deployed (e.g. recommender systems, self-driving cars, healthcare), and where the computational, economic and environmental cost of re-training a complex policy can be high and serve as barrier to inclusivity. However, forgoing finetuning on the target task can come at the cost of safety concerns during deployment in real-world settings, e.g. human-robot interaction or treatment administration to patients. We thus encourage future works in this area to mitigate the issues outlined above through a safety analysis.

References

- [1] A. Agarwal, M. Henaff, S. Kakade, and W. Sun. Pc-pg: Policy cover directed exploration for provable policy gradient learning. In *NeurIPS*, 2020.
- [2] R. Agarwal, M. C. Machado, P. S. Castro, and M. G. Bellemare. Contrastive behavioral similarity embeddings for generalization in reinforcement learning. In *ICLR*, 2021.
- [3] A. Anand, E. Racah, S. Ozair, Y. Bengio, M.-A. Côté, and R. D. Hjelm. Unsupervised state representation learning in atari. In *NeurIPS*, 2019.
- [4] Y. M. Asano, C. Rupprecht, and A. Vedaldi. Self-labelling via simultaneous clustering and representation learning. *ICLR*, 2020.
- [5] M. Azabou, M. G. Azar, R. Liu, C.-H. Lin, E. C. Johnson, K. Bhaskaran-Nair, M. Dabagia, K. B. Hengen, W. Gray-Roncal, M. Valko, and E. L. Dyer. Mine your own view: Self-supervised learning through across-sample prediction, 2021.
- [6] P. Bachman, R. D. Hjelm, and W. Buchwalter. Learning representations by maximizing mutual information across views. In *NeurIPS*, 2019.
- [7] A. Barreto, W. Dabney, R. Munos, J. J. Hunt, T. Schaul, H. Van Hasselt, and D. Silver. Successor features for transfer in reinforcement learning. *arXiv preprint arXiv:1606.05312*, 2016.
- [8] M. Bucher, S. Herbin, and F. Jurie. Generating visual representations for zero-shot classification. In *Proceedings of the IEEE International Conference on Computer Vision Workshops*, pages 2666–2673, 2017.
- [9] M. Caron, I. Misra, J. Mairal, P. Goyal, P. Bojanowski, and A. Joulin. Unsupervised learning of visual features by contrasting cluster assignments. In *NeurIPS*, 2020.
- [10] P. S. Castro. Scalable methods for computing state similarity in deterministic markov decision processes. In *AAAI*, volume 34, pages 10069–10076, 2020.
- [11] T. Chen, S. Kornblith, M. Norouzi, and G. Hinton. A simple framework for contrastive learning of visual representations. In *ICML*, 2020.
- [12] K. Cobbe, C. Hesse, J. Hilton, and J. Schulman. Leveraging procedural generation to benchmark reinforcement learning. In *ICML*, 2020.
- [13] K. Cobbe, J. Hilton, O. Klimov, and J. Schulman. Phasic policy gradient. *arXiv preprint arXiv:2009.04416*, 2020.
- [14] M. Cuturi. Sinkhorn distances: Lightspeed computation of optimal transportation distances. In *NeurIPS*, 2013.
- [15] W. Dabney, A. Barreto, M. Rowland, R. Dadashi, J. Quan, M. G. Bellemare, and D. Silver. The value-improvement path: Towards better representations for reinforcement learning. In *AAAI*, 2021.
- [16] B. Eysenbach, A. Gupta, J. Ibarz, and S. Levine. Diversity is all you need: Learning skills without a reward function. In *ICLR*, 2019.

[17] N. Ferns, P. Panangaden, and D. Precup. Metrics for finite markov decision processes. In *UAI*, volume 4, pages 162–169, 2004.

[18] C. Gelada, S. Kumar, J. Buckman, O. Nachum, and M. G. Bellemare. Deepmdp: Learning continuous latent space models for representation learning. In *ICML*, pages 2170–2179. PMLR, 2019.

[19] J.-B. Grill, F. Strub, F. Altché, C. Tallec, P. H. Richemond, E. Buchatskaya, C. Doersch, B. A. Pires, Z. D. Guo, M. G. Azar, B. Piot, K. Kavukcuoglu, R. Munos, and M. Valko. Bootstrap your own latent: A new approach to self-supervised learning. In *NeurIPS*, 2020.

[20] A. Gupta, B. Eysenbach, C. Finn, and S. Levine. Unsupervised meta-learning for reinforcement learning. *arXiv preprint arXiv:1806.04640*, 2018.

[21] K. He, H. Fan, Y. Wu, S. Xie, and R. Girshick. Momentum contrast for unsupervised visual representation learning. In *CVPR*, 2020.

[22] R. D. Hjelm, A. Fedorov, S. Lavoie-Marchildon, K. Grewal, P. Bachman, A. Trischler, and Y. Bengio. Learning deep representations by mutual information estimation and maximization. In *ICLR*, 2018.

[23] M. Jaderberg, V. Mnih, W. M. Czarnecki, T. Schaul, J. Z. Leibo, D. Silver, and K. Kavukcuoglu. Reinforcement learning with unsupervised auxiliary tasks. *ICLR*, 2017.

[24] A. Kendall, J. Hawke, D. Janz, P. Mazur, D. Reda, J.-M. Allen, V.-D. Lam, A. Bewley, and A. Shah. Learning to drive in a day. In *ICRA*, 2019.

[25] S. Levine, C. Finn, T. Darrell, and P. Abbeel. End-to-end training of deep visuomotor policies. *Journal of Machine Learning Research*, 17(39):1–40, 2016. URL <http://jmlr.org/papers/v17/15-522.html>.

[26] B. Li, V. François-Lavet, T. Doan, and J. Pineau. Domain adversarial reinforcement learning. *arXiv preprint arXiv:2102.07097*, 2021.

[27] B. Mazoure, R. T. des Combes, T. Doan, P. Bachman, and R. D. Hjelm. Deep reinforcement and infomax learning. In *NeurIPS*, 2020.

[28] D. Misra, M. Henaff, A. Krishnamurthy, and J. Langford. Kinematic state abstraction and provably efficient rich-observation reinforcement learning. In *International conference on machine learning*, pages 6961–6971. PMLR, 2020.

[29] V. Mnih, K. Kavukcuoglu, D. Silver, A. A. Rusu, J. Veness, M. G. Bellemare, A. Graves, M. Riedmiller, A. K. Fidjeland, G. Ostrovski, S. Petersen, C. Beattie, A. Sadik, I. Antonoglou, H. King, D. Kumaran, D. Wierstra, S. Legg, and D. Hassabis. Human-level control through deep reinforcement learning. *Nature*, 518(7540):529–533, Feb. 2015. ISSN 00280836. URL <http://dx.doi.org/10.1038/nature14236>.

[30] J. Oh, S. Singh, H. Lee, and P. Kohli. Zero-shot task generalization with multi-task deep reinforcement learning. In *International Conference on Machine Learning*, pages 2661–2670. PMLR, 2017.

[31] E. Perez, F. Strub, H. de Vries, V. Dumoulin, and A. Courville. Film: Visual reasoning with a general conditioning layer. In *AAAI*, 2018.

[32] R. Raileanu and R. Fergus. Decoupling value and policy for generalization in reinforcement learning. In *ICML*, 2021.

[33] K. Rakelly, A. Zhou, C. Finn, S. Levine, and D. Quillen. Efficient off-policy meta-reinforcement learning via probabilistic context variables. In *ICML*, pages 5331–5340. PMLR, 2019.

[34] P. J. Rousseeuw. Silhouettes: a graphical aid to the interpretation and validation of cluster analysis. *Journal of computational and applied mathematics*, 20:53–65, 1987.

[35] J. Schulman, F. Wolski, P. Dhariwal, A. Radford, and O. Klimov. Proximal policy optimization algorithms, 2017.

[36] M. Schwarzer, A. Anand, R. Goel, R. D. Hjelm, A. Courville, and P. Bachman. Data-efficient reinforcement learning with self-predictive representations. In *ICLR*, 2021.

[37] S. Sohn, J. Oh, and H. Lee. Hierarchical reinforcement learning for zero-shot generalization with subtask dependencies. *arXiv preprint arXiv:1807.07665*, 2018.

[38] A. Srinivas, M. Laskin, and P. Abbeel. Curl: Contrastive unsupervised representations for reinforcement learning. In *ICML*, 2020.

[39] A. Stooke, K. Lee, P. Abbeel, and M. Laskin. Decoupling representation learning from reinforcement learning, 2020.

[40] T. Sylvain, L. Petrini, and D. Hjelm. Locality and compositionality in zero-shot learning. In *ICLR*, 2020.

[41] A. Touati and Y. Ollivier. Learning one representation to optimize all rewards. In *ICLR Self-supervision for Reinforcement Learning Workshop*, 2021.

[42] A. van den Oord, Y. Li, and O. Vinyals. Representation learning with contrastive predictive coding, 2019.

[43] B. Van Roy and Z. Wen. Generalization and exploration via randomized value functions. In *ICML*, 2016.

[44] C. Villani. *Optimal transport: old and new*, volume 338. Springer Science & Business Media, 2008.

[45] J. Wu, T. Zhang, Z.-J. Zha, J. Luo, Y. Zhang, and F. Wu. Self-supervised domain-aware generative network for generalized zero-shot learning. In *CVPR*, pages 12767–12776, 2020.

[46] M. Yang and O. Nachum. Representation matters: Offline pretraining for sequential decision making. In *ICLR*, 2021.

[47] D. Yarats, R. Fergus, A. Lazaric, and L. Pinto. Reinforcement learning with prototypical representations. In *ICML*, 2021.

[48] A. Zhang, S. Sodhani, K. Khetarpal, and J. Pineau. Learning robust state abstractions for hidden-parameter block mdps. In *ICLR*, 2020.

[49] A. Zhang, R. McAllister, R. Calandra, Y. Gal, and S. Levine. Learning invariant representations for reinforcement learning without reconstruction. In *ICLR*, 2021.

8 Appendix

8.1 Experiment details

Name	Description	Value
γ	Discount factor	0.999
λ	Decay	0.95
$n_{\text{timesteps}}$	Number of timesteps per rollout	256
n_{epochs}	Number of epochs for RL and representation learning	1
n_{samples}	Number of samples per epoch	8192
Entropy bonus	Entropy loss coefficient	0.01
Clip range	Clip range for PPO	0.2
Learning rate	Learning rate for RL and representation learning	5×10^{-4}
Number of environments	Number of parallel environments	32
Optimizer	Optimizer for RL and representation learning	Adam
Frame stack	Frame stack X Procgen frames	1
E	Number of clusters	200
k	Number of k-NN nearest neighbors	3
T	Number of clustering timesteps	2
β	Clustering temperature	0.3

Table 3: Experiments’ parameters

We implemented all algorithms on top of the IMPALA architecture, which was shown to perform well on Procgen [12]. In the Procgen experiments, ProtoRL was ran without any intrinsic rewards (since the domains are not exploration-focused) by first jointly training the representation and RL losses for 8M timesteps, after which only the RL loss was optimized for an additional 8M steps (16M steps in total). Similarly, DIAYN was also run with the pre-training phase of 8M and then RL only objective for the second 8M phase.

We used NVIDIA Tesla P40 GPUs for all our experiments, the codebase of which is based on the OpenAI implementation of Procgen baselines.

8.2 Pseudocode

Algorithm 1: Cross Trajectory Representation Learning

Inputs :online encoder ϕ , cluster projector θ_{clust} , cluster encoder ψ_{clust} , mining projector θ_{pred} , mining encoder ψ_{pred} , cluster basis matrix \mathbf{E}

Hyperparameters : B – trajectory batch size, C – num. of trajectory clusters, T – subtrajectory length, K – num. of nearest clusters for view mining, L – trajectory length, N – num. of anchors for view mining, β – Sinkhorn temperature

```

1 for each iteration  $itr = 1, 2, \dots$  do
2   for each minibatch  $\mathcal{B}$  do
3     for each trajectory  $\tau_i$  in  $\mathcal{B}$  do
4        $t_1, \dots, t_T \sim \text{Uniform}(L)$  // Sample temporal keypoints
5        $u^{(\tau_i)} = [FiLM(\phi(s_{t_1}), a_{t_1}), \dots, FiLM(\phi(s_{t_T}), a_{t_T})]$ 
6       // cluster dynamics
7        $\mathbf{u}_i = [u^{(\tau_1)}, \dots, u^{(\tau_m)}]$  // batch dynamics
8        $\mathbf{v}_i = \psi_{\text{clust}}(\mathbf{u}_i)$  // fetch embeddings
9        $\mathbf{w}_i = \theta_{\text{clust}}(\mathbf{v}_i)$  // fetch projections
10       $\mathbf{v}_i = \frac{\mathbf{v}_i}{\|\mathbf{v}_i\|_2}$  // normalize embeddings
11       $\mathbf{Q} = \text{Softmax}(\mathbf{v}_i^\top \mathbf{E} / \beta)$  // Compute latent dynamics scores
12       $\tilde{\mathbf{Q}} = \text{Sinkhorn}(\mathbf{Q})$  // normalize scores through Sinkhorn
13       $\mathbf{P} = \log[\text{Softmax}(\mathbf{w}_i^\top \mathbf{E} / \beta)]$  // Compute projected dynamics scores
14       $\mathcal{L}_{\text{clust}}(\phi, \psi_{\text{clust}}, \theta_{\text{clust}}) = \text{CrossEntropy}(\tilde{\mathbf{Q}}, \mathbf{P})$ 
15      // Predicting neighbors
16       $\mathbf{D}_{ij} = \|\mathbf{e}_i - \mathbf{e}_j\|_2^2$  // find pairwise basis distances
17       $\mathcal{L}_{\text{pred}} = 0$ 
18      for each anchor  $j = 1, \dots, N$  do
19         $\tau_j \sim \mathcal{B}$  // Sample anchor trajectory
20         $\mathbf{u}_n = u^{(\tau_j)}$  // Set anchor embedding
21         $c_i^{(1)}, \dots, c_i^{(k)} = \text{top-knn}(\mathbf{D}, k, c_i)$  // Find nearby clusters
22         $u_{c_1}, \dots, u_{c_k} \sim p(u_{c_i^{(1)}}), \dots, p(u_{c_i^{(k)}})$  // Sample views from clusters
23         $\mathbf{v}'_{c_1}, \dots, \mathbf{v}'_{c_K} = \psi_{\text{pred}}(u_{c_1}), \dots, \psi_{\text{pred}}(u_{c_K})$  // embed mined views
24         $\mathbf{w}'_n = \theta_{\text{pred}}(\psi_{\text{pred}}(\mathbf{u}_n))$  // mining target
25         $\mathcal{L}_{\text{pred}}^{(n)} = \sum_{k=1}^K \|\mathbf{w}'_n - \text{StopGrad}(\mathbf{v}'_{c_k})\|_2^2$ 
26         $\mathcal{L}_{\text{pred}} = \sum_{n=1}^N \mathcal{L}_{\text{pred}}^{(n)}$ 
27         $\mathcal{L}_{\text{CTRL}} = \mathcal{L}_{\text{clust}} + \mathcal{L}_{\text{pred}}$  // update networks
28         $\phi, \psi_{\text{clust}}, \theta_{\text{clust}}, \theta_{\text{pred}}, \psi_{\text{pred}} = \text{Adam}(\phi, \psi_{\text{clust}}, \theta_{\text{clust}}, \theta_{\text{pred}}, \psi_{\text{pred}}; \mathcal{L}_{\text{CTRL}})$ 
29      for each minibatch  $\mathcal{B}$  do
30         $\pi, V^\pi = \text{Adam}(\pi, V^\pi; \mathcal{L}_{\text{RL}}(\mathcal{B}))$  // update RL parameters

```

8.3 Additional results

Ablations on algorithm components We ran multiple versions of the algorithm to identify the key components which make CTRL perform well in Procgen. The first modification, **CTRL consecutive** T consists in running our algorithm but sampling consecutive timesteps, that is $t_{i+1} = t_1 + i$ for all t_1 and $0 \leq i \leq T$. The second modification, **CTRL no action** removes the action conditioning layer in the log-softmax probability p_t and in the cluster scores q_t , to test the importance of action information for cluster membership prediction. The third modification, **CTRL no cluster** removes the clustering loss, and only restricts to mining and predicting nearby neighbors in the batch. Finally, the last

modification, **CTRL no pred** removes the loss predicting samples from neighboring partitions and only relies on the clustering loss to update its representation.

Table 4: Average evaluation returns collected after 8M of training frames, \pm one standard deviation.

Env	CTRL consecutive T	CTRL no action	CTRL no cluster	CTRL no pred
bigfish	3.9 \pm 0.3	3.2 \pm 0.3	2.5 \pm 0.3	3.7 \pm 0.1
bossfight	8.9 \pm 0.1	6.9 \pm 0.9	7.8 \pm 0.3	6.6 \pm 0.8
caveflyer	4.6 \pm 0.2	4.7 \pm 0.1	4.6 \pm 0.1	4.6 \pm 0.1
chaser	7.4 \pm 0.3	6.7 \pm 0.2	7.0 \pm 0.5	6.5 \pm 0.1
climber	6.2 \pm 0.4	5.5 \pm 0.1	5.3 \pm 0.4	5.7 \pm 0.4
coinrun	8.8 \pm 0.1	8.5 \pm 0.3	8.1 \pm 0.2	8.4 \pm 0.3
dodgeball	1.8 \pm 0.1	1.7 \pm 0.1	1.7 \pm 0.2	1.7 \pm 0.1
fruitbot	13.1 \pm 0.3	12.9 \pm 0.4	13.0 \pm 0.5	12.5 \pm 0.6
heist	3.0 \pm 0.1	3.2 \pm 0.3	3.2 \pm 0.1	3.0 \pm 0.2
jumper	6.1 \pm 0.2	6.0 \pm 0.1	5.9 \pm 0.1	5.9 \pm 0.1
leaper	3.4 \pm 1.1	3.2 \pm 0.4	2.6 \pm 0.3	2.7 \pm 0.2
maze	5.6 \pm 0.2	5.6 \pm 0.1	5.7 \pm 0.1	5.8 \pm 0.1
miner	7.0 \pm 0.9	5.9 \pm 0.4	5.6 \pm 0.1	6.0 \pm 0.2
ninja	5.7 \pm 0.1	5.3 \pm 0.2	5.5 \pm 0.1	5.5 \pm 0.1
plunder	6.4 \pm 0.2	5.6 \pm 0.1	5.9 \pm 0.5	6.1 \pm 0.2
starpilot	7.0 \pm 0.2	4.9 \pm 0.6	4.9 \pm 0.2	5.0 \pm 0.4

Results suggest that (1) using consecutive timesteps as for the dynamics vector embedding yields lower average rewards than non-consecutive timesteps, (2) action conditioning helps the agent to pick up on the local dynamics present in the MDP and (3) both clustering and predictive objectives are essential to the good performance of our algorithm.

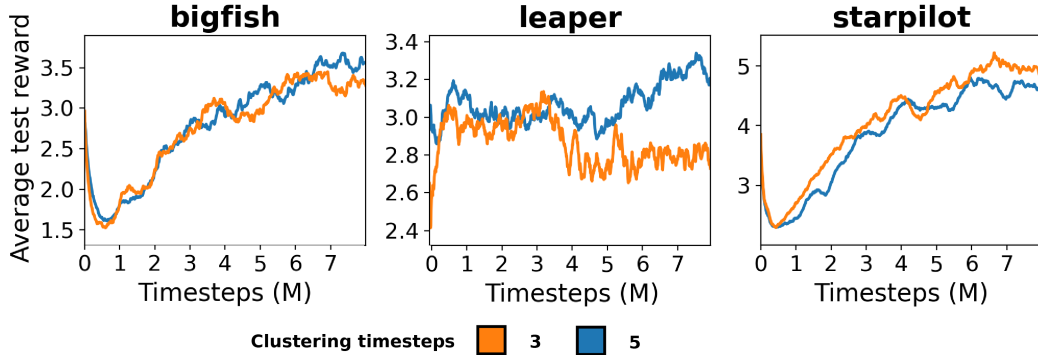


Figure 4: Ablation on the clustering timesteps used in the dynamics embedding

Ablation on number of clusters and clustering timesteps

Temporal connectivity of the clusters Are clusters *consistent* in time for a given trajectory? To verify this, we trained CTRL on 1 million frames of the *bigfish* game. For every T states in a given trajectory, we have computed the hard cluster assignment to the nearest cluster, which yields a sequence of partitions. We then computed the cosine similarity between time-adjacent cluster centroids, the metric reported on the smoothed graph below.

Loss landscape of $\mathcal{L}_{\text{clust}}$ and $\mathcal{L}_{\text{pred}}$ Works relying on non-collinear signals, e.g. behavioral similarity and rewards, as is the case for DeepMDP [18], show that interference can occur between various loss components. For example, [18] showed how their dynamics and reward losses are inversely proportional to each other early on in the training, taking a considerable amount of frames to converge.

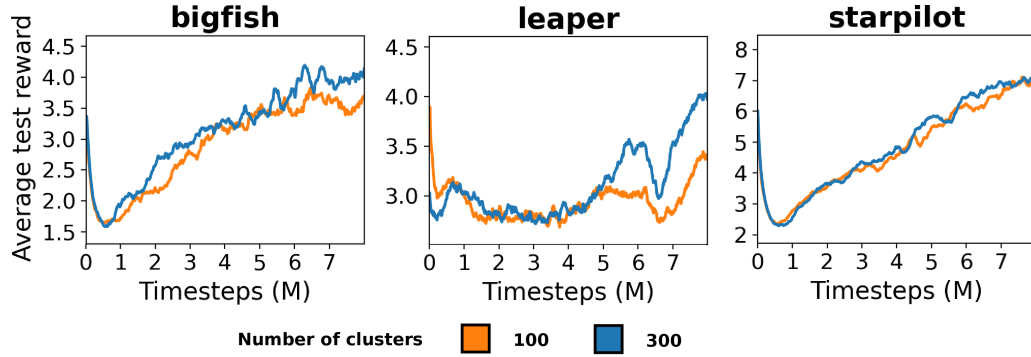


Figure 5: Ablation on the number of clusters used in CTRL

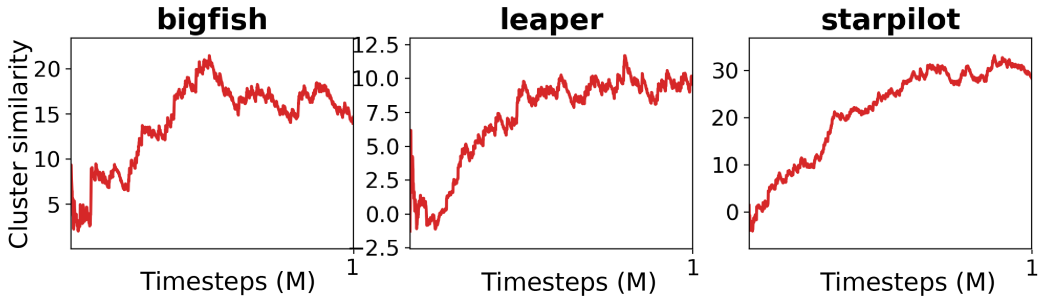


Figure 6: Average within-trajectory cluster similarity over 1M consecutive timesteps.

We observe a similar pattern in Figure 7: the clustering loss first jumps up while the predictive loss is minimized, then the trend reverses, and both losses get minimized near the end of the training.

Case study: splitting other dynamics-aware losses Similar to the postulate of ATC [39], we hypothesize that training the encoder only with the representation loss has the most beneficial effect when the representation loss contains information about dynamics. To validate this, we conducted an additional set of experiments on two well-known self-supervised learning algorithms which leverage predictive information about future timesteps: Deep Reinforcement and InfoMax Learning (DRIML) [27] and Self-Predictive Representations (SPR) [36]. We ran (i) the default version of the algorithms with joint RL and representation updates, as well as (ii) RL updates propagated only through the layers above the encoder.

8.4 Additional theoretical findings

Do uncorrelated local changes to state embeddings affect the clustering?

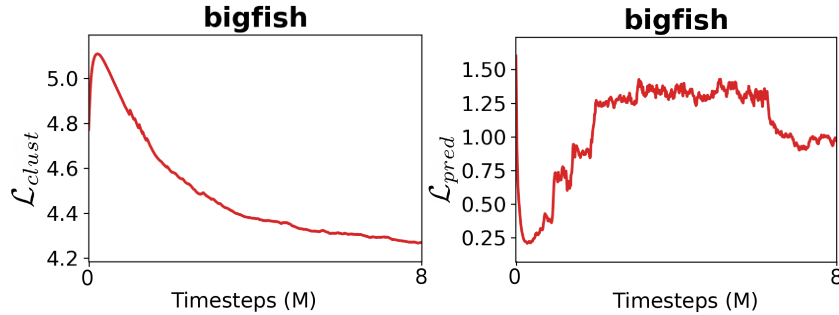


Figure 7: Average values of \mathcal{L}_{clust} and \mathcal{L}_{pred} over time.

Env		DRIML	SPR
bigfish		+0.17	+0.15
bossfight		+0.56	+10.36
caveflyer		+0.23	-0.02
chaser		-0.14	-0.13
climber		0.15	+0.14
coinrun		-0.37	+2.05
dodgeball		-0.39	+0.12
fruitbot		-0.53	-0.1
heist		-0.3	-0.03
jumper		+0.04	+0
leaper		-0.04	+0.08
maze		+0.01	-0.15
miner		+0.88	+0.03
ninja		-0.13	-0.31
plunder		-0.02	-0.18
starpilot		-0.11	-0.15
Norm. score		+0.01	+0.74

Table 5: Normalized improvement scores of split updates over joint updates of the encoder, averaged over 3 random seeds.

Theorem 8.1 *Let M be an MDP and let $\mathbf{v} \in \mathcal{V}$ be a dynamics embeddings in M . Define*

$$\begin{cases} \boldsymbol{\delta}_i = \boldsymbol{\delta}_i^1 & 1 \leq i \leq |\mathcal{V}| \\ \boldsymbol{\delta}_i = \boldsymbol{\delta}_i^2 & h < i \leq T|\mathcal{V}| \end{cases} \quad (9)$$

and pick $\boldsymbol{\delta}^1$ s.t. it lies on the positive half-plane spanned by $\mathbf{E}_j^\top - \mathbf{E}_{j'}^\top$ for some $1 \leq j' \leq E$. Then, $\mathbf{v}' = \mathbf{v} + \boldsymbol{\delta}$ and \mathbf{v} belong to the same partition j .

It becomes apparent from the above statement that perturbations to a single state or groups of state embeddings *do not* modify the partition membership as long as their direction aligns with that of the cluster embeddings.

8.5 Proofs

Throughout this section, we assume that the policy π is fixed, and that CTRL optimizes \mathcal{L}_{clust} only.

Proof 1 (Theorem 8.1) *For two dynamics embeddings to be assigned to the same cluster j , the following should hold*

$$\begin{aligned} \sum_{i=1}^{|\mathcal{V}|} \mathbf{v}_i \mathbf{E}_{ji}^\top &> \sum_{i=1}^{|\mathcal{V}|} \mathbf{v}_i \mathbf{E}_{j'i}^\top, \\ \sum_{i=1}^{|\mathcal{V}|} (\mathbf{v}_i + \boldsymbol{\delta}_i) \mathbf{E}_{ji}^\top &> \sum_{i=1}^{|\mathcal{V}|} (\mathbf{v}_i + \boldsymbol{\delta}_i) \mathbf{E}_{j'i}^\top \end{aligned} \quad (10)$$

for any $1 \leq j' \leq E$ s.t. $j' \neq j$.

$$\begin{aligned} \sum_{i=1}^{|\mathcal{V}|} \mathbf{v}_i \mathbf{E}_{ji}^\top + \sum_{i=1}^{|\mathcal{V}|} \boldsymbol{\delta}_i \mathbf{E}_{ji}^\top &> \sum_{i=1}^{|\mathcal{V}|} \mathbf{v}_i \mathbf{E}_{j'i}^\top + \sum_{i=1}^{|\mathcal{V}|} \boldsymbol{\delta}_i \mathbf{E}_{j'i}^\top \\ \sum_{i=1}^{|\mathcal{V}|} \mathbf{v}_i (\mathbf{E}_{ji}^\top - \mathbf{E}_{j'i}^\top) + \sum_{i=1}^{|\mathcal{V}|} \boldsymbol{\delta}_i (\mathbf{E}_{ji}^\top - \mathbf{E}_{j'i}^\top) &> 0 \end{aligned} \quad (11)$$

Taking the difference between both equations yields the necessary condition for two dynamics to belong to the same cluster

$$\sup_{1 \leq j' \leq E} (\mathbf{E}_{ji}^\top - \mathbf{E}_{j'i}^\top) \boldsymbol{\delta}_i \geq 0, \quad 1 \leq i \leq |\mathcal{V}|. \quad (12)$$

Corollary 8.1.1 Let \mathbf{v}, \mathbf{v}' be two dynamics embeddings, and define $\boldsymbol{\delta} = \mathbf{v}' - \mathbf{v}$. If \mathbf{v} belongs to cluster j and $j = \arg \max_{1 \leq j' \leq E} \mathbf{E}_{j'}^\top \boldsymbol{\delta}$, then \mathbf{v}' also belongs to cluster j .

Perturbations are of the form $\sum_{i=1}^{|\mathcal{V}|} (\mathbf{E}_{ij}^\top - \mathbf{E}_{ij'}^\top) \boldsymbol{\delta}_i$. If $\boldsymbol{\delta} = 0$, then the cluster assignment doesn't change. Let \mathbf{v} be of size $kh = |\mathcal{V}|$. Define, without loss of generality

$$\begin{cases} \boldsymbol{\delta}_i = \boldsymbol{\delta}_i^1 & 1 \leq i \leq h \\ \boldsymbol{\delta}_i = \boldsymbol{\delta}_i^2 & h < i \leq kh \end{cases} \quad (13)$$

and pick $\boldsymbol{\delta}^1$ s.t. it lies on the positive half-plane spanned by $\mathbf{E}_{ij}^\top - \mathbf{E}_{ij'}^\top$.

Then,

$$\sum_{i=1}^{|\mathcal{V}|} (\mathbf{E}_{ij}^\top - \mathbf{E}_{ij'}^\top) \boldsymbol{\delta}_i = \sum_{i=1}^h (\mathbf{E}_{ij}^\top - \mathbf{E}_{ij'}^\top) \boldsymbol{\delta}_i^1 + \sum_{i=h}^{kh} (\mathbf{E}_{ij}^\top - \mathbf{E}_{ij'}^\top) \boldsymbol{\delta}_i^2 \geq \sum_{i=h}^{kh} (\mathbf{E}_{ij}^\top - \mathbf{E}_{ij'}^\top) \boldsymbol{\delta}_i^2 \geq 0 \quad (14)$$

which concludes the proof.

Proof 2 (Theorem 1) Since the \mathcal{W}_1 metric is defined between distribution functions, we use $\mathbf{v} = \mathbb{P}[\mathbf{v}]$ throughout the proof to denote the probability distribution over elements of the dynamics vector \mathbf{v} . In practice, this amounts to re-normalizing the representation.

For two dynamics to be assigned to the same cluster j , the following has to hold:

$$\begin{aligned} \sum_{i=1}^{|\mathcal{V}|} \mathbf{v}_i \mathbf{E}_{ji}^\top &> \sum_{i=1}^{|\mathcal{V}|} \mathbf{v}_i \mathbf{E}_{j'i}^\top, \\ \sum_{i=1}^{|\mathcal{V}|} \mathbf{v}'_i \mathbf{E}_{ji}^\top &> \sum_{i=1}^{|\mathcal{V}|} \mathbf{v}'_i \mathbf{E}_{j'i}^\top \end{aligned} \quad (15)$$

for any $1 \leq j' \leq E$ s.t. $j' \neq j$. Then, adding both inequalities yields, for all $1 \leq j \leq E$

$$\begin{aligned} \sum_{i=1}^{|\mathcal{V}|} \mathbf{v}_i \mathbf{E}_{ji}^\top + \sum_{i=1}^{|\mathcal{V}|} \mathbf{v}'_i \mathbf{E}_{ji}^\top &\geq \sum_{i=1}^{|\mathcal{V}|} \mathbf{v}_i \mathbf{E}_{j'i}^\top + \sum_{i=1}^{|\mathcal{V}|} \mathbf{v}'_i \mathbf{E}_{j'i}^\top \\ \sum_{i=1}^{|\mathcal{V}|} \mathbf{v}_i \mathbf{E}_{ji}^\top + \sum_{i=1}^{|\mathcal{V}|} \mathbf{v}_i \mathbf{E}_{j'i}^\top &\geq \sum_{i=1}^{|\mathcal{V}|} \mathbf{v}'_i \mathbf{E}_{ji}^\top + \sum_{i=1}^{|\mathcal{V}|} \mathbf{v}'_i \mathbf{E}_{j'i}^\top \\ \sum_{i=1}^{|\mathcal{V}|} \mathbf{v}_i (\mathbf{E}_{ji}^\top - \mathbf{E}_{j'i}^\top) &\geq \sum_{i=1}^{|\mathcal{V}|} \mathbf{v}'_i (\mathbf{E}_{ji}^\top - \mathbf{E}_{j'i}^\top) \\ \sum_{i=1}^{|\mathcal{V}|} \mathbf{v}_i (\mathbf{E}_{ji}^\top - \mathbf{E}_{j'i}^\top) &\geq \sum_{i=1}^{|\mathcal{V}|} \mathbf{v}'_i (\mathbf{E}_{ji}^\top - \mathbf{E}_{j'i}^\top) \end{aligned} \quad (16)$$

and the constraint of two vectors belonging to the same cluster j becomes

$$\begin{aligned} \sum_{i=1}^{|\mathcal{V}|} (\mathbf{v}_i - \mathbf{v}'_i) (\mathbf{E}_{ji}^\top - \mathbf{E}_{j'i}^\top) &\geq 0 \\ \max_{1 \leq j' \leq E} \sum_{i=1}^{|\mathcal{V}|} (\mathbf{v}_i - \mathbf{v}'_i) (\mathbf{E}_{ji}^\top - \mathbf{E}_{j'i}^\top) &\geq 0 \\ \max_{1 \leq j' \leq E} (\mathbf{v} - \mathbf{v}') (\mathbf{E}_j - \mathbf{E}_{j'})^\top &\geq 0 \end{aligned} \quad (17)$$

Now, denote $\mathbf{E}(j) := \mathbf{E}_j$. Our constraint satisfaction problem can be written as

$$\max_{1 \leq j' \leq E} (\mathbf{v} - \mathbf{v}')(\mathbf{E}(j) - \mathbf{E}(j'))^\top \geq 0 \quad (18)$$

By comparing Eq. 8 with Eq. 18, we observe that in our case, μ is restricted to the set of vectors in $\mathbb{R}^{|\mathcal{V}|}$. Therefore, we pick $\mu \in \Gamma(\mathbf{E})$, where $\Gamma(\mathbf{E}) = \{\omega \in \mathcal{V} : \omega = \mathbf{E}(j, i) - \mathbf{E}(j', i), 0 \leq \omega_i \leq 1, \cos(\mathbf{v} - \mathbf{v}', \omega) \in [0, \pi] | 1 \leq i \leq |\mathcal{V}|, 1 \leq j' \leq E\}$. The set $\Gamma(\mathbf{E})$ is non-empty if $\max_{l, l'} \|\mathbf{E}_l - \mathbf{E}_{l'}\|_\infty \leq 1$, which holds due to ℓ_p norm ordering and since \mathbf{E} is normalized in the $\tilde{\mathbf{Q}}$ scores expression. Adopting this notation simplifies the previous expression to

$$\max_{\mu \in \Gamma(\mathbf{E})} (\mathbf{v} - \mathbf{v}')\mu^\top \quad (19)$$

Once again, recall that \mathbf{E} is normalized. Therefore, we have

$$\left(\frac{\mathbf{e}_{ij}}{\|\mathbf{e}_j\|_2} - \frac{\mathbf{e}_{i'j}}{\|\mathbf{e}_j\|_2} \right) + \left(\frac{\mathbf{e}_{ij}}{\|\mathbf{e}_j\|_2} - \frac{\mathbf{e}_{i'j'}}{\|\mathbf{e}_j\|_2} \right) \leq d(i, i') \quad (20)$$

which equivalently can be re-stated as (for $e_i \geq e_j$ WLOG):

$$\begin{aligned} \mathbf{e}_{ij} - \mathbf{e}_{i'j} &\leq \frac{\|\mathbf{e}_j\|_2}{2} d(i, i') \\ \mathbf{e}_{ij} - \mathbf{e}_{i'j} &\leq \frac{\|\mathbf{e}_j\|_2^2}{2} (\mathbf{E}_{ij} - \mathbf{E}_{i'j}) \\ \mathbf{e}_{ij} - \mathbf{e}_{i'j} &\leq \frac{\|\mathbf{e}_j\|_2}{2} (\mathbf{e}_{ij} - \mathbf{e}_{i'j}), \end{aligned} \quad (21)$$

where we take, as an example, $d(i, i') = \|\mathbf{e}_j\|_2 (\mathbf{E}_{ij} - \mathbf{E}_{i'j})$.

The final expression for the sufficient condition for two dynamics embeddings to belong to the same partition is

$$\begin{aligned} \max_{\mu \in \Gamma(\mathbf{E})} (\mathbf{v} - \mathbf{v}')\mu^\top \\ \text{s.t. } \mu(i) - \mu(i') \leq d(i, i') \end{aligned} \quad (22)$$

for $d(i, i') = \|\mathbf{e}_j\|_2 (\mathbf{E}_{ij} - \mathbf{E}_{i'j})$, which is similar to the Wasserstein-1 distance under d , i.e. $\mathcal{W}_1^d(\mathbf{v}, \mathbf{v}')$.

We constructed an operator similar to $\mathcal{F}(d)$ in [17]. d can be computed by recursively applying $\mathcal{F}(d)$ at each $\mathbf{v}, \mathbf{v}' \in \mathcal{V}$ pointwise, which is similar to what is done in CTRL. This concludes our proof and shows how our clustering procedure can be viewed as finding reward-free bisimulations.

However, note that the exact interpretation of reward-free bisimulation relation depends on how \mathbf{v} is defined. Taking \mathbf{v} to be two consecutive timesteps of state-action pairs yields the closest possible to the original definition of bisimulation, while sampling temporal keypoints far across the trajectory will induce a different set of properties.